

## Electronic Supplementary Information (ESI)

### Diffusion of single dye molecules in hydrated TiO<sub>2</sub> mesoporous films

Juan F. Angiolini<sup>1</sup>, Martín Stortz<sup>2</sup>, Paula Y. Steinberg<sup>3</sup>, Esteban Mocoskos<sup>4</sup>, Luciana Bruno<sup>5</sup>, Galo Soler-Illia<sup>6</sup>, Paula C. Angelomé<sup>3</sup>, Alejandro Wolosiuk<sup>3,7\*</sup>, and Valeria Levi<sup>1,\*</sup>

#### 1. TiO<sub>2</sub>-based MOTF synthesis

TiO<sub>2</sub>-based MOTF were prepared by a combination of sol-gel and Evaporation Induced Self Assembly (EISA) techniques from a sol containing an inorganic precursor and an organic pore template.<sup>1</sup> The sol was prepared as reported in previous works<sup>1</sup> by mixing TiCl<sub>4</sub> (Sigma Aldrich) and absolute ethanol (EtOH, BIOPACK) in a 1:40 molar ratio. The pore template Brij58®([CH<sub>3</sub>(CH<sub>2</sub>)<sub>15</sub>(CH<sub>2</sub>CH<sub>2</sub>O)<sub>20</sub>OH], Merck) or Pluronic F127 ([HO(CH<sub>2</sub>CH<sub>2</sub>O)<sub>106</sub>(CH<sub>2</sub>CH(CH<sub>3</sub>)O)<sub>70</sub>(CH<sub>2</sub>CH<sub>2</sub>O)<sub>106</sub>H], Sigma Aldrich) and E-pure H<sub>2</sub>O (R = 18MΩ.cm<sup>-1</sup>) were added to the mixture. The final molar compositions were 1 TiCl<sub>4</sub>: 40 EtOH: 10 H<sub>2</sub>O: 0.05 Brij58 and 1 TiCl<sub>4</sub>: 40 EtOH: 10 H<sub>2</sub>O: 0.005 F127.

Substrates were cleaned with ethanol before thin film deposition. The as prepared sol was deposited onto glass substrates by dip-coating at 2 mm s<sup>-1</sup> withdrawal speed inside a camera at *ca.* 30 % relative humidity (RH) and at room temperature. These materials were stabilized and calcined in consecutive steps. The stabilization steps consisted of 24 h in a chamber at 50% RH and at room temperature, 24 h at 60°C and 24 h at 130°C. All the systems were finally treated at the following calcination temperatures 350 or 400°C during 2 h with a ramp of 1°C min<sup>-1</sup> from 130°C. Surfactant extracted samples were first treated at 200°C during 2 h with a ramp of 1°C min<sup>-1</sup> from 130°C and later immersed in EtOH for 48 h before measurements.

#### 2. Characterization of TiO<sub>2</sub> – MOTF films

##### a) Transmission electron microscopy (TEM)

TEM images were collected using a Philips EM 301 transmission electron microscope operated at 60 kV. Samples were obtained by scratching the films from the substrate

with a razor blade and dispersed in ethanol. A drop of the ethanolic dispersion was deposited on a carbon-coated copper grid and dried before analysis.

### b) Bidimensional Small-Angle X-ray Scattering (2D-SAXS)

2D-SAXS analysis confirmed the pore symmetry of the TiO<sub>2</sub>-MOTF frameworks. The measurements were performed at the SAXS2 beamline at the Laboratório Nacional de Luz Síncrotron (LNLS, Campinas, SP, Brazil). A  $\lambda = 1.55 \text{ \AA}$  was selected and the data collection was performed with a CCD detector. Figure S1 shows the obtained bidimensional patterns.

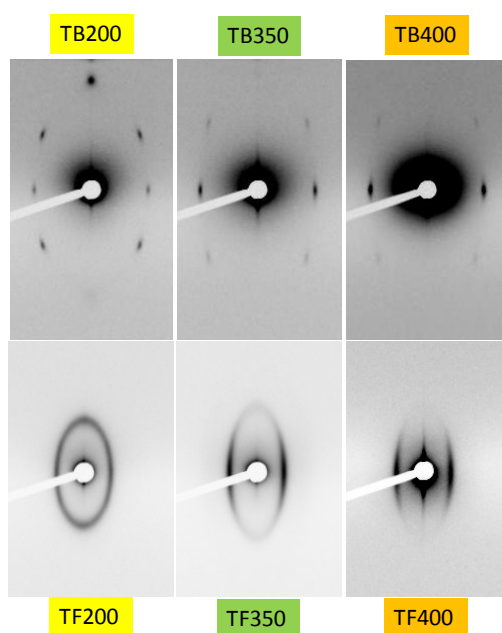


**Figure S1:** 2D-SAXS patterns of the samples, as indicated in the labels

For the TB family, the obtained structure is body centered cubic  $Im3m$  with the [110] plane parallel to the substrate. The same structure is obtained for the TF family, with some degree of disorder also present. The thermal treatment contracts the structure in the direction parallel to the substrate, evidenced by the elongation of the 2D-SAXS pattern in the  $y$  direction.<sup>2,3</sup>

### c) Fourier Transform Infra-Red spectroscopy (FTIR).

To confirm the correct template elimination, FTIR measurements were performed in a Nicolet Magna 560 instrument equipped with liquid N<sub>2</sub> cooled MCT-A detector. A drop of each sol was deposited onto a KBr pellet, and treated in the same way for the TiO<sub>2</sub>-

MOTF synthesis. Measurements were made at different stages of the thermal and extraction treatments. Figure S2 presents the results obtained for TF family.

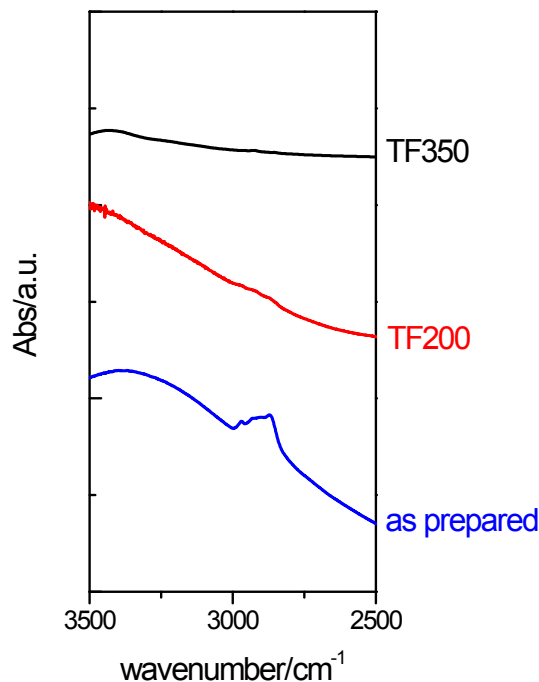


**Figure S2:** FTIR spectra in the  $\nu_{CH}$  region for TF samples, as indicated in the labels.

Typical IR absorption bands attributed to the C-H vibrations of the surfactant template ( $\sim 3000 - 2800 \text{ cm}^{-1}$  region) are evident in the as prepared films. After either thermal or extraction treatment the IR absorbance signal strongly decays. However, in the latter case some signal can be observed, suggesting that a small amount of template remains in the samples.

#### **d) Environmental Ellipsometric Porosimetry (EEP)**

Porosity and pore size distribution were obtained by EEP.<sup>4, 5</sup> Water adsorption-desorption curves were measured in a SOPRA GES5A equipment. Film thickness and refractive index values were obtained from the ellipsometric parameters  $\Psi$  and  $\Delta$  under dry air flux containing variable water vapor pressure,  $P$ ;  $P/P_0$  was varied from 0 to 1 ( $P_0$  being the saturation water vapor pressure at 25 °C). Water volume adsorbed at each  $P/P_0$  value was determined by modeling the obtained refractive index according to a three-component (water-air-oxide) Bruggeman effective medium approximation. Adsorption-desorption isotherms were obtained by plotting the water volume adsorbed by the porous film at each  $P/P_0$ . The pore size distributions were determined using models based on the Kelvin equation on these isotherms, taking into

account the water contact angle in the film. The adsorption branch of the EEP curves was used to calculate the pore size and the desorption branch was used to calculate the necks sizes.<sup>6, 7</sup> The contact angle of water on the films was determined by depositing a sessile droplet directly on top of the sample and captured the static contact angle using a Ramé-Hart 290-F4. Image analysis was performed with Ramé-Hart DROP image software. Figure S3 presents the obtained EEP results for the TB family. The contact angles used to calculate the pore and neck sizes are presented in Table S1.

**Table S1.** H<sub>2</sub>O contact angle measurements for TiO<sub>2</sub>-MOTF

<b>Sample</b>	<b>H<sub>2</sub>O contact angle (°)</b>
TB200	50
TB350	10
TB400	26
TF200	41
TF350	15
TF400	16

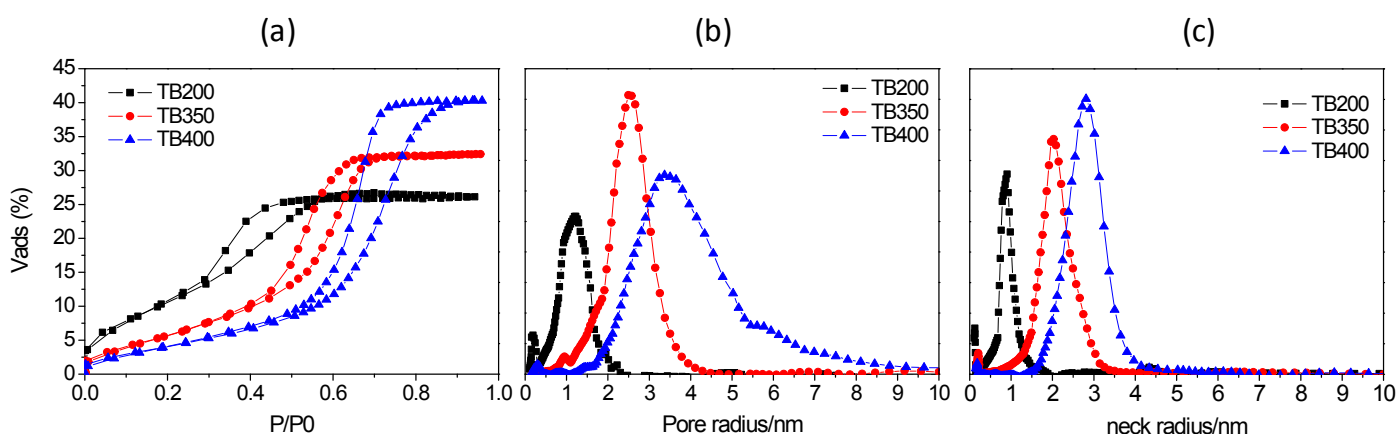


**Figure S3.** Experimental EEP curves for TB TiO<sub>2</sub>-MOTF family, as indicated in the labels (a), pore radius distribution (b) and neck radius distribution (c).

The results indicate that the porosity of the samples increases when the temperature of the thermal treatment is incremented; the same tendency is observed for the pore and neck sizes. Similar results were obtained for the TF family (not shown). This behavior is related with the structure contraction observed by 2D-SAXS: at higher temperature, more collapse in the direction perpendicular to the substrate occurs. This contraction is accompanied by stiffening of the titania walls and more connection between the pores. These results have been previously reported by our group.<sup>2, 8</sup>

Regarding the H<sub>2</sub>O contact angles, it can be seen that the samples treated at 350°C and 400°C are highly hydrophilic. In the case of samples treated at 200°C, in which the elimination of the template was performed by extraction, higher contact angles are obtained, suggesting that a small amount of the surfactant may have remained in the pores, as seen from FTIR results. However, it is important to make clear that all the samples are hydrophilic, and it is expected they are fully filled with water under the fluorescence measurements conditions (RH ~ 93%).

#### e) X-ray diffraction (XRD)

XRD patterns were recorded on a Panalytical Empyrean diffractometer, using Cu K $\alpha$  radiation (1.54 Å), 1° incident beam angle, a 0.38 mm divergence slit and a 15 mm mask. A monochromator was positioned between the sample and the detector. Diffraction patterns were collected from 22.5 to 28° (2 $\theta$ ) with a step size of 0.025° and time per step of 5 seconds. The chosen range corresponds to (101) reflection of anatase.

Figure S4 presents the results obtained for TB family. Equivalent results were obtained for TF films.

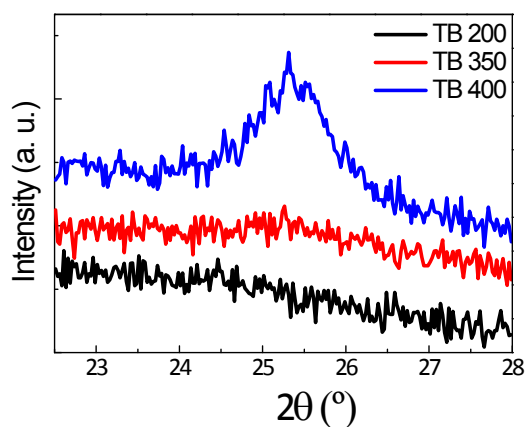
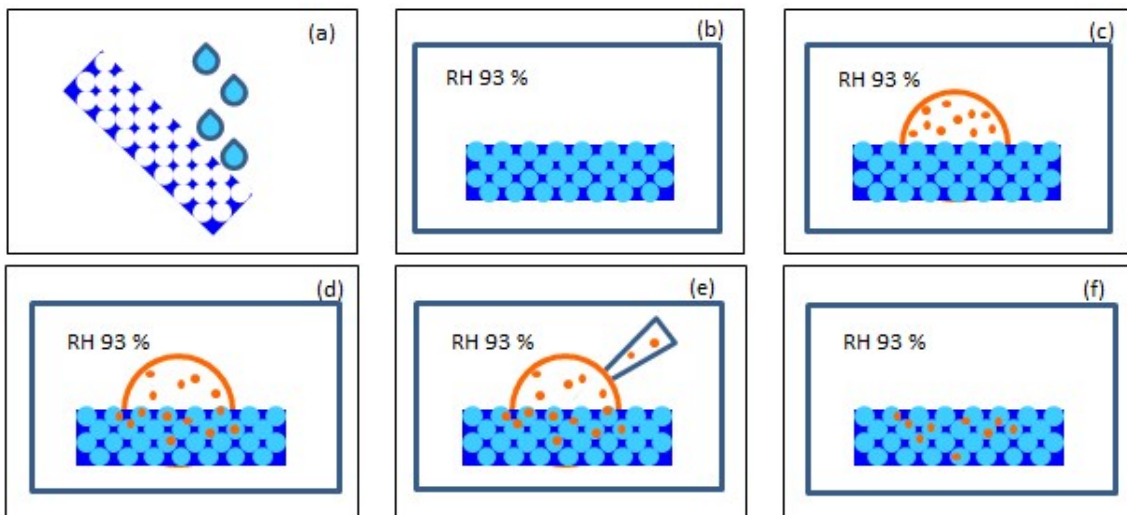


**Figure S4.** XRD patterns from TB samples treated at different temperatures, as indicated in the labels.

XRD results demonstrate that anatase crystals are present in the samples treated at the higher temperature (400°C), while the samples treated at lower temperatures are amorphous. These results are in agreement with previously reported tendencies for samples prepared onto glass substrates.<sup>9</sup>

### **3. Incorporation of Rhodamine B into hydrated TiO<sub>2</sub> films**

Rhodamine B dye was obtained from Sigma-Aldrich (purity >95%) and was used without further purification. Calcined and surfactant-extracted TiO<sub>2</sub> thin films were first rinsed with EtOH and DI H<sub>2</sub>O; afterwards they were placed in a humidity-controlled chamber containing a saturated solution of KNO<sub>3</sub> (~93 % relative humidity, RH) for 1 h.<sup>10</sup> Then, 50 μL of a 50 nM Rhodamine B solution in 20 mM Tris (pH = 8) was placed on top of the films during 2-5 minutes at 93 % RH. Later, the dye solution was removed from the TiO<sub>2</sub> film surface and the film was left overnight at 93% RH. This process assures the full hydration of the pores and dye diffusion while avoiding the presence of an aqueous solution layer on top of the film<sup>2</sup>. The ionic strength of the dye solutions was adjusted with NaCl.



**Scheme 1.** Representative steps for the procedure of Rhodamine B infiltration within the TiO<sub>2</sub>-MOTF: TiO<sub>2</sub>-MOTF films rinsing with H<sub>2</sub>O and ethanol (a), 1 hour in closed chamber with 93% RH (b), 50  $\mu$ L of highly diluted Rhodamine B solution is deposited on top for 2 – 5 minutes (c-d), removal of the dye solution (e) and the film is left overnight in order to allow dye diffusion (f).

#### 4. *Microscopy confocal imaging*

Confocal imaging was performed in a laser scanning confocal microscope Olympus FV1000 (Olympus, Japan) using a 60X NA 1.35 oil-immersion objective. Rhodamine B was excited using a He-Ne green laser (543 nm, average power at the sample, 700 nW). Fluorescence was collected in the range 606-695 nm and detected with a photomultiplier set in the pseudo photon-counting detection mode. The pixel size was set at 83 nm. Measurements were performed in a custom-made PDMS cell with a small reservoir for a saturated KNO<sub>3</sub> solution in order to keep the relative humidity at 93%.

#### 5. *Fluorescence recovery after photobleaching (FRAP)*

FRAP measurements were carried out in a FV1000 confocal microscope (Olympus, Japan) using a 60X NA 1.35 oil-immersion objective. A strip of 20  $\mu$ m x 4  $\mu$ m was then photobleached by repetitively scanning the laser (30  $\mu$ W, 8.5 frames/s) for 23 s.

The laser power was then reduced to 300 nW and the fluorescence recovery was followed by repetitively imaging (1.02 frames/s) a 42 x 42  $\mu$ m<sup>2</sup> region of interest containing the photobleached region. The pixel size was 165 nm. The intensity at the

bleached region was corrected for photobleaching during imaging and used to construct the recovery curve as described previously<sup>11, 12</sup>.

The following, empirical equation was fitted to the recovery curve:

$$FRAP(t) = \sum_{i=1}^n A_i (1 - e^{-t/\tau_i}) \quad (S1)$$

where  $A_i$  is the amplitude of each component,  $t$  represents time after photobleaching and  $\tau_i$  the time constant of each component. The mobile fraction (Mf) was calculated as:

$$Mf = \frac{F_{\infty} - F_0}{F_i - F_0} \quad (S2)$$

where  $F_i$  is the intensity prior to the photobleaching step,  $F_0$  the fluorescence intensity immediately after photobleaching and  $F_{\infty}$  is the intensity at the end of the FRAP experiment.

The Mf value reported in this work is the mean  $\pm$  standard error obtained from 12 independent measurements.

## 6. Fluorescence correlation spectroscopy

FCS measurements were performed in the FV1000 confocal microscope with the detector set in photon counting mode using a 60X NA 1.35 oil-immersion objective. The laser power at the sample was set to 300 nW. The fluorescence intensity was collected at a frequency of 100000 Hz during 90 s and used to calculate the autocorrelation function as:

$$G(\tau) = \frac{\langle I(t) \cdot I(t + \tau) \rangle}{\langle I(t) \rangle^2} \quad (S3)$$

where  $I(t)$  is the fluorescence intensity and  $\tau$  is a lag time.

Equation (1) was fit to the experimental autocorrelation function to obtain  $\tau_D$ . This value was used to estimate the diffusion coefficient of the probe as<sup>13</sup>:

$$D = \frac{\sigma_0^2}{4\tau_D} \quad (S4)$$

were  $\omega_0$  is the axial waist of the confocal observation volume ( $0.26 \pm 0.01 \mu\text{m}$ ,  $N = 5$ ) and was estimated using a reference solution of Rhodamine B in a 50% glycerol solution ( $D = 73 \mu\text{m}^2/\text{s}$ ).

Between 7 to 30 independent FCS measurements were run in each experimental condition.

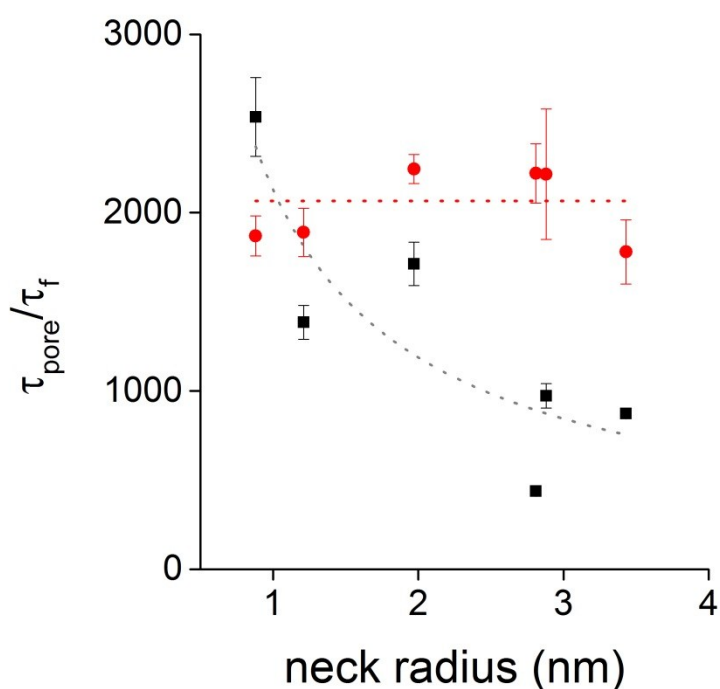
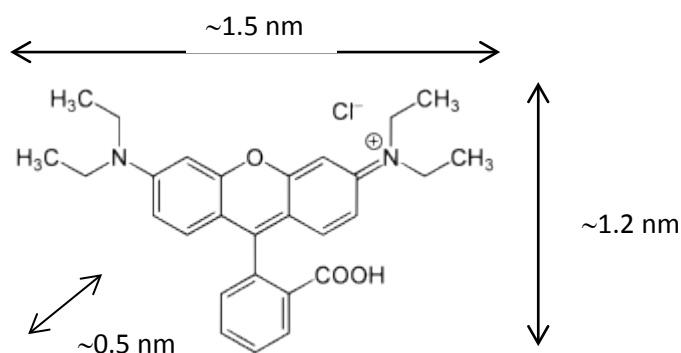


**Figure S5.** Relative dwell time of the probe at single pores at low (●) and high (■) ionic strength. The error bars represent the standard error of the data. Dotted lines were included only to facilitate the observation of the data.  $\tau_{\text{pore}}/\tau_f$  decreases with the pore size at high ionic strength revealing an increase in the escape probability. On the other hand, at low ionic strength, the relative dwell time in the pore is high and approximately constant suggesting that the pore geometry does not affect the escape probability in this condition.

## 7. Molecular modeling

Approximate molecular dimensions of Rhodamine B, shown in Scheme S2, were obtained from Avogadro open-source software package (v 1.2.0).<sup>14</sup>



**Scheme S2.** Molecular structure of Rhodamine B and approximate molecular dimensions.

### Supplementary references

1. E. L. Crepaldi, G. J. D. A. A. Soler-Illia, D. Grosso, F. Cagnol, F. Ribot and C. Sanchez, *Journal of the American Chemical Society*, 2003, **125**, 9770-9786.
2. G. J. A. A. Soler-Illia, P. C. Angelomé, M. C. Fuertes, D. Grosso and C. Boissiere, *Nanoscale*, 2012, **4**, 2549-2566.
3. E. L. Crepaldi, G. J. A. A. Soler-Illia, D. Grosso, F. Cagnol, F. Ribot and C. Sánchez, *J. Am. Chem. Soc.*, 2003, **125**, 9770-9786.
4. M. R. Baklanov, K. P. Mogilnikov, V. G. Polovinkin and F. N. Dultsev, *Journal of Vacuum Science and Technology B: Microelectronics and Nanometer Structures*, 2000, **18**, 1385-1391.
5. A. Bourgeois, A. Brunet-Bruneau, S. Fisson, J. Rivory, M. Matheron, T. Gacoin and J. P. Boilot, *Adsorption*, 2005, **11**, 195-199.
6. C. Boissiere, D. Grosso, S. Lepoutre, L. Nicole, A. B. Bruneau and C. Sanchez, *Langmuir*, 2005, **21**, 12362-12371.
7. M. C. Fuertes, M. Marchena, M. C. Marchi, A. Wolosiuk and G. J. A. A. Soler-Illia, *Small*, 2009, **5**, 272-280.
8. I. L. Violi, M. D. Perez, M. C. Fuertes and G. J. A. A. Soler-Illia, *ACS Appl. Mater. Interfaces*, 2012, **4**, 4320-4330.
9. P. C. Angelomé, L. Andrini, M. E. Calvo, F. G. Requejo, S. A. Bilmes and G. J. A. A. Soler-Illia, *J. Phys. Chem. C*, 2007, **111**, 10886-10893.
10. L. Greenspan, *J Res Natl Bur Stand Sect A Phys Chem*, 1977, **81 A**, 89-96.
11. D. Axelrod, D. E. Koppel, J. Schlessinger, E. Elson and W. W. Webb, *Biophys J*, 1976, **16**, 1055-1069.

12. D. M. Soumpasis, *Biophys J*, 1983, **41**, 95-97.
13. E. L. Elson, *Methods Enzymol*, 2013, **518**, 11-41.
14. M. D. Hanwell, D. E. Curtis, D. C. Lonie, T. Vandermeersch, E. Zurek and G. R. Hutchison, *Journal of Cheminformatics*, 2012, **4**.